Growth, microstructure, and magnetic properties of highly textured and highly coercive Nd-Fe-B films

Volker Neu,* Steffen Melcher, Ullrich Hannemann, Sebastian Fähler, and Ludwig Schultz
IFW Dresden, Institute for Metallic Materials, Helmholtzstrasse 20, D-01069 Dresden, Germany
(Received 24 April 2004; published 29 October 2004)

Thin Nd-Fe-B films have been prepared by pulsed laser deposition on sapphire substrates. A Ta buffer layer has been used to promote epitaxial growth. The deposition temperature has been varied between 400 °C and 700 °C and proved to be an important parameter for both, the phase formation and the control of microstructure and coercivity. For low temperatures the Nd-Fe-B films grow in small grains with irregular shape, and the generally observed *c*-axis texture is not fully developed. The coercivity reaches values of around 1.6 T. For medium preparation temperatures of 600–650 °C the Nd-Fe-B films grow in small rectangular grains which are mostly isolated from each other. Maximum coercivities of 1.9 T together with in-plane to out-of-plane remanence ratios as low as 0.05 have been achieved. These films possess a nearly perfect magnetic texture with the easy magnetization axis perpendicular to the film plane. For higher deposition temperatures the microstructure coarsens substantially and also oxidation of Nd occurs. Additionally, the coercivity drops drastically. Optimally prepared films have been investigated by magnetic force microscopy. The perfect growth of the $Nd_2Fe_{14}B$ phase and the special granular microstructure allow us to study the domain structure of isolated, single crystalline $Nd_2Fe_{14}B$ grains on a submicrometer scale. The observed domain patterns show stripe domains, which are typical for films with large perpendicular magnetic anisotropy, and resemble the specific shape of the magnetic grains. The domain width varies from 100 to 300 nm depending on the grain height and can, on a first approximation, be described by domain theory of extended films.

DOI: 10.1103/PhysRevB.70.144418 PACS number(s): 75.70.Kw, 68.37.Rt, 75.60.Jk, 75.70.Ak

I. INTRODUCTION

Permanent magnet films with specialized magnetic performance are required in the key applications of today's trend for microstructured devices. This concerns the field of magnetic microelectromechanical systems, microstructured magnetic sensors or logic devices, and also the field of magnetic data storage.

Since some years the magnetic material which dominates the high performance bulk magnets market—$Nd_2Fe_{14}B$—can be deposited with a sufficient quality to be attractive for magnetic films.[1,2] As usual for magnetic materials, the microstructure has to transfer the intrinsic potential of the magnetic phase into useful extrinsic properties, and, therefore, requires appropriate processing. Two different approaches are commonly used for preparation.[3] The first approach uses deposition at ambient temperature and a postannealing procedure in order to form the $Nd_2Fe_{14}B$ phase. That way, isotropic films with coercivities between 1 T and 2.5 T are typically obtained.[4] In order to enhance the remanence above 50% of the saturation magnetization—the limit for uncoupled isotropic films—films with small, exchange-coupled grains are prepared by a short-time annealing procedure.[5] An additional increase in remanence is obtained by exchange-coupled multilayers or nanocomposites consisting of the highly anisotropic $Nd_2Fe_{14}B$ phase and materials with a high saturation magnetization as Fe (Refs. 6 and 7) or Fe-Co.[8] These multiphase systems, however, only achieve coercivities up to 1.5 T. The second approach uses heated substrates, on which the $Nd_2Fe_{14}B$ phase is formed directly upon deposition.[9–13] In most cases this leads to a texture where the *c* axis (the easy magnetization axis) is oriented perpendicular to the substrate. Though this in principle allows remanences comparable to the saturation magnetization, the extended time during which the film is kept at high temperatures makes it difficult to control grain growth and interdiffusion. As a consequence this often leads to low coercivities. Another approach, which combines the two above mentioned methods, proved to be interesting.[14] The deposition of Nd-Fe-B at an intermediate temperature of 300 °C is followed by a postannealing step. Due to this procedure, a good texture together with a reasonable coercivity of 1.6 T is obtained. Currently it is not clear, whether the texture evolves by the growth of small oriented nuclei created during the first deposition step,[14,15] or by a directed crystallization originating at an interface.[4,16,17]

Due to the large differences in the preparation routes it is still under discussion which microstructure is necessary for good extrinsic magnetic properties. Whereas for postannealed films a small grain size is crucial, for films deposited on a heated substrate no clear picture exists. Measurements of the domain structure of Nd-Fe-B films are quite challenging because of rough and irregular microstructures or small grain sizes. This often leads to interaction domains, which render it difficult to interpret magnetic contrast.[18,19] Therefore, a detailed understanding of the correlation between microstructure and magnetic properties in thin Nd-Fe-B films is still missing.

Recently, thin Nd-Fe-B films could be prepared on heated substrates, which combine an almost perfect out-of-plane texture with coercivities of up to 2.0 T.[20] One reason for these outstanding magnetic properties is an epitaxial growth of Nd-Fe-B on a special buffer system that enables the desired good texture and the perfect formation of the $Nd_2Fe_{14}B$ phase with unaltered intrinsic properties. Another reason is a special granular microstructure, which arises from a low wet-

tability of $Nd_2Fe_{14}B$ on the buffer material. Due to the high fraction of surface, these granular films now allow one to investigate the correlation between topographic and magnetic microstructure. The thorough study of the growth and the (magnetic) microstructure of these highly textured and highly coercive Nd-Fe-B films is the topic of this paper. Special attention is given to the role of the substrate temperature on the microstructure and magnetic domain structure and its influence on the magnetic properties.

After listing the experimental details of preparation and measurements the results and their interpretation are summarized in different sections. Section III A describes the phase formation of the films with the help of x-ray diffraction (XRD) measurements. Investigations of phases and microstructure via atomic force microscopy (AFM) and scanning electron microscopy (SEM) follow in Sec. III B. In Sec. III C the magnetic properties as a function of substrate temperature are given. A detailed understanding of the magnetic behavior is obtained by a study of the magnetic microstructure of different samples via magnetic force microscopy (MFM). These investigations are summarized in Sec. III D. This section also includes a comparison of the observed domain structures and their characteristic length scales with the domain theory of magnetic films with strong perpendicular magnetic anisotropy.

II. EXPERIMENT

Thin Nd-Fe-B films were deposited in an UHV chamber (base pressure $=10^{-9}$ mbar) using pulsed laser deposition. A KrF laser beam was directed by a mirror/lens system into the vacuum chamber and an aperture in the beam line was imaged onto the targets resulting in a homogeneous energy density of about 5 J/cm^2. The targets were elemental Fe and Nd foils and a $Fe_{54}B_{46}$ alloy, which were alternately moved into the laser beam to deposit films with the desired composition. The target-substrate distance was 40 mm. Prior to film deposition the deposited mass per pulse was measured for each target with an Inficon XTM/2 rate monitor. Based on the pulse ratio necessary for stoichiometric $Nd_2Fe_{14}B$, the number of pulses onto the Nd target was increased by a factor of 4 to compensate Nd losses and to obtain a Nd-rich composition, which allows a decoupling of the $Nd_2Fe_{14}B$ grains. The substrate temperature was monitored with an Impac IGA 120 pyrometer. A 100 nm thick Ta buffer layer was deposited on the heated sapphire substrate prior to the Nd-Fe-B film deposition.[21] To prevent the films from oxidation they were covered *in situ* with a 100 nm Cr layer at a temperature below 250 °C.[22] The thickness of cold deposited and, therefore, smooth reference films was determined to be (200 ± 30) nm by measuring across a deposition edge with a Dektak 3030 ST alpha stepper. Microstructural investigations were performed with a digital instruments Dimension 3100 AFM in tapping mode, a JEOL 6400 SEM and a high-resolution LEO 1530 FEGSEM. X-ray θ-2θ scans were measured with a Siemens D5000 diffractometer utilizing Co-K_α radiation. The magnetic properties were measured with a quantum design ACMS P500 in dc mode. The composition was determined by glow discharge optical emission spectroscopy. The overall stoichiometry turned out to be $Nd_{27}Fe_{57}B_{16}$, which is equivalent to a Nd:Fe-ratio of about 1:2 rather than 1:7 for the stoichiometric $Nd_2Fe_{14}B$ phase. In terms of a two-phase microstructure it can be referred to as 59 vol % $Nd_2Fe_{14}B+41$ vol % Nd (disregarding the small B surplus). This interpretation is motivated by the known phase diagram of Nd-Fe-B, where the $Nd_2Fe_{14}B$ phase exists only in a very small homogeneity range.

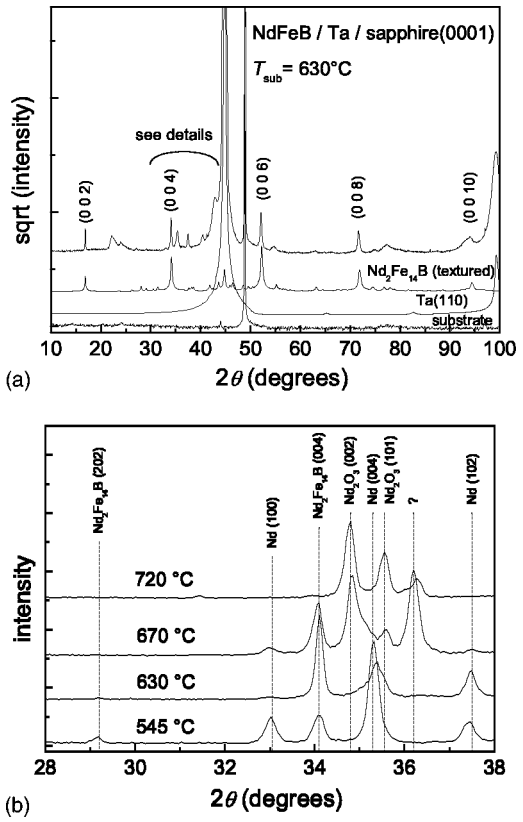

FIG. 1. (a) Typical θ-2θ scan of a Nd-Fe-B film deposited at 630 °C on Ta/sapphire with predominantly $Nd_2Fe_{14}B(001)$ peaks, and (b) peak details for films prepared at different temperatures revealing additional phases.

III. RESULTS AND DISCUSSION

A. Phase formation

Figure 1(a) shows a typical XRD pattern of a Nd-Fe-B film deposited at 630 °C on a Ta buffered sapphire substrate together with a measured substrate pattern and calculated Ta and $Nd_2Fe_{14}B$ patterns for comparison. Ta grows on sapphire with a (110) orientation and the signal from the $Nd_2Fe_{14}B$ phase is dominated by the (001) reflections. The formation of the $Nd_2Fe_{14}B$ phase was confirmed for deposition temperatures up to 700 °C. The enlarged section of the diffraction pattern [Fig. 1(b)] reveals the detailed evolution of the $Nd_2Fe_{14}B$ phase with deposition temperature and also the presence of additional phases. For the lowest deposition temperature (545 °C) the $Nd_2Fe_{14}B$ (202) peak is also visible, for higher temperatures only (001) reflections are present. This indicates a preferred orientation of the *c* axis, which is

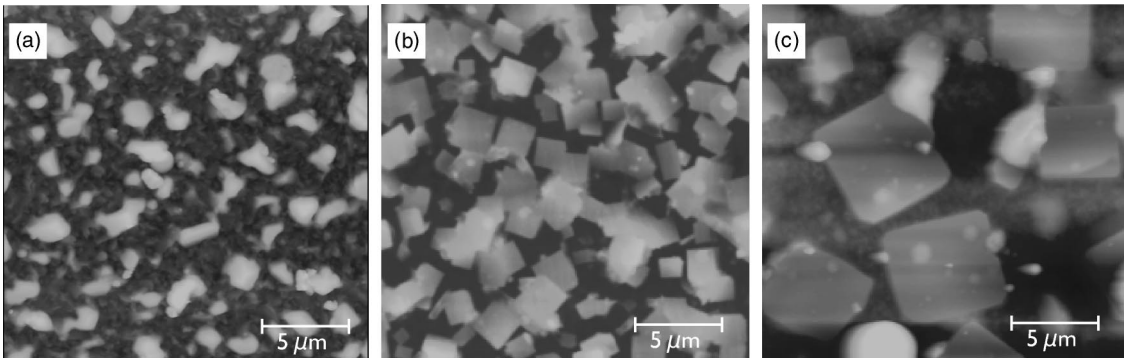

FIG. 2. AFM images of Nd-Fe-B films prepared at (a) 545 °C, (b) 630 °C, and (c) 670 °C.

the easy magnetization axis of the tetragonal unit cell, perpendicular to the film. The maximum intensity for 2:14:1 reflections is observed at a deposition temperature of 630 °C. For films deposited above 700 °C no reflections of the $Nd_2Fe_{14}B$ phase are found. Besides $Nd_2Fe_{14}B$ reflections one observes diffraction lines identified as elemental Nd in accordance to the overall Nd-rich composition. These lines are clearly visible for films prepared at low temperatures (545 °C). They decrease in intensity for increasing temperature and almost vanish for deposition at 670 °C. Simultaneously, reflections which can be indexed as Nd_2O_3 appear in the diffraction pattern. At the highest temperature (720 °C) only Nd-oxide peaks and an unidentified reflection remain. In summary, we observe the formation of the hard magnetic $Nd_2Fe_{14}B$ phase with a pronounced *c*-axis texture, which deteriorates with a too low deposition temperature. This texture is promoted by the reported epitaxy of $Nd_2Fe_{14}B$ on Ta.[20] On the other hand, an increasing deposition temperature leads to strong oxidation of Nd, both of the elemental Nd phase and of the Nd bound in the $Nd_2Fe_{14}B$ phase. Earlier x-ray photoemission spectroscopy experiments indicate that the oxidation originates from a failure of the Ta buffer to prevent oxygen diffusion out of the ceramic substrate. Consequently, too high deposition temperatures result in a complete destruction of the hard magnetic phase.

B. Microstructure

The microstructure dependence on the deposition temperature is illustrated in Fig. 2. At 545 °C the films show a rather inhomogeneous morphology with small, "edgy" grains of about 500 nm size in the background and larger, irregularly shaped grains with a size of around 1–2 μm on top of the smaller grains. At 630 °C the morphology is dominated by almost square-shaped grains, which grow on a flat surface and are densely packed. The size of these grains ranges from 1 to 3 μm. For samples prepared at higher temperatures rectangular but also edgy grains are loosely distributed on the surface. These grains are significantly larger (up to 10 μm) and have a much wider size distribution compared to those observed at 630 °C. Again, some irregularly shaped grains are found on top of the rectangular grains.

To correlate the morphological features with the phases identified by XRD for the above shown samples, AFM measurements are compared with SEM measurements. This allows chemical identification either by composition contrast in the backscattering mode (BSE) or direct energy dispersive x-ray analysis (EDX) measurements. Figure 3(a) shows a SEM image of the sample prepared at 545 °C. EDX measurements were performed at five different positions as indicated in the image. The composition in position 1 is richest in Cr and Ta and has a Nd:Fe ratio of about 1:2.5. This is close to the ratio of the overall composition measured on the film. Therefore, it is concluded that the background consists of a mixture of small $Nd_2Fe_{14}B$ and Nd grains, which cannot be resolved laterally, embedded between the Ta buffer and the Cr cover layer. The large and irregularly shaped grains such as at spots 2 and 3 give a smaller Cr and Ta signal but possess a large Nd:Fe ratio of 1.5:1. Concluding from the XRD results we identify them as Nd grains. However, not all grains having similar morphology when observed by SEM or AFM are Nd-rich. The grains denoted as 4 and 5 yield a similarly low Ta and Cr signal but are, on the other hand, Fe rich (Nd:Fe=1:4.5). This ratio does not equal exactly the value for $Nd_2Fe_{14}B$, but, considering the typical diameter of 1 μm which is probed by EDX, these grains are identified as $Nd_2Fe_{14}B$. The Nd-Fe-B film prepared at 630 °C has also been investigated with SEM, as described in detail in Ref. 23. There, the square-shaped grains, of which almost the whole film consists, could be identified as $Nd_2Fe_{14}B$. Although the grains are densely packed, a large number of them is still separated by Nd or a Nd-rich phase. Part of the Ta buffer was not covered at all, indicating a low wettability of $Nd_2Fe_{14}B$ and Nd on Ta. The height of these grains, as

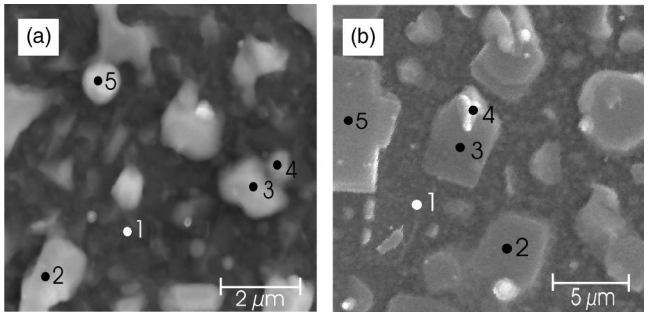

FIG. 3. Scanning electron micrographs (secondary electron contrast) of two Nd-Fe-B films deposited at (a) 545 °C and (b) 670 °C. Composition analysis has been performed with EDX at the marked positions.

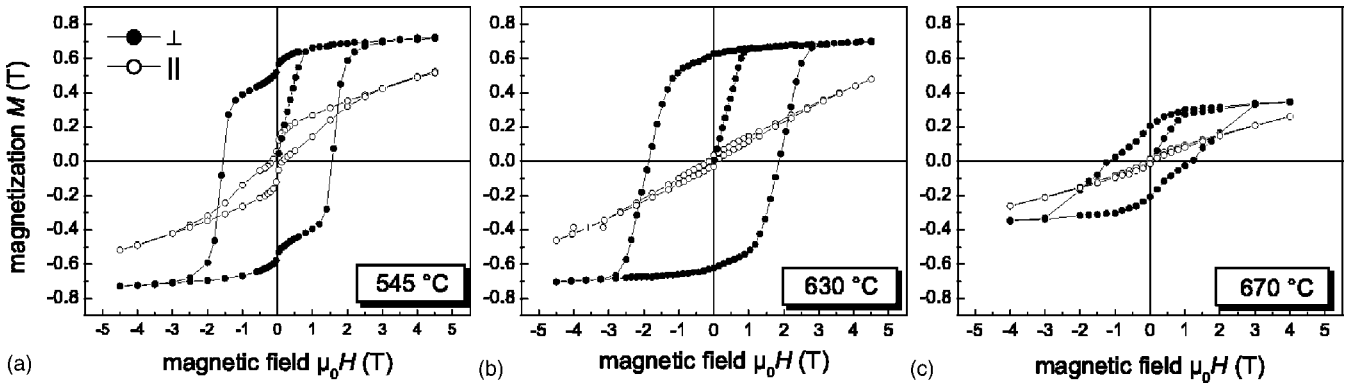

FIG. 4. Magnetic hysteresis measured perpendicular and parallel to the film plane for three Nd-Fe-B films deposited at (a) 545 ° C, (b) 630 °C, and (c) 670 °C.

measured by AFM, is of the order of the overall film thickness. For an even higher deposition temperature of 670 °C the grains grow larger and are, to a large extent, isolated. Again, the majority of grains possesses a rectangular shape but there are also some taller, less regularly shaped grains. Their morphology and the positions which are used for EDX analysis are illustrated in Fig. 3(b). The composition in position 1 is again dominated by Cr and Ta, and there is no Nd found in the region between the clearly visible grains. The rectangular grains (as in positions 2 and 3) possess a lower amount of Cr and Ta and a Nd:Fe ratio of 1:7, as expected for the $Nd_2Fe_{14}B$ phase. The large size of these grains allows a more reliable determination of the composition without an interfering signal from neighboring grains. The height of these grains is about 100–400 nm. The irregularly shaped grains (position 4) are mainly found on top of Nd-Fe-B grains and possess a high Nd content (Nd:Fe ratio=1:1). They are again identified as Nd grains. Apparently, the already mentioned low wettability of Nd on Ta avoids pure Nd growing on Ta directly, especially at higher temperatures. Not completely understood are grains as found at position 5. Their shape is similar to $Nd_2Fe_{14}B$ grains but the Nd:Fe ratio of 1:3 is far too Nd rich for a pure $Nd_2Fe_{14}B$ phase. The stoichiometry suggests the $Nd_{1.1}Fe_4B_4(\eta)$ phase, but this cannot be confirmed by x-ray diffraction. These grains appear frequently in samples prepared at higher temperatures and are typically very large (10–30 μm).

C. Macroscopic magnetic properties

The hysteresis curves for the samples deposited at 545 °C, 630 °C, and 670 °C are depicted in Fig. 4. The out-of-plane measurements are not corrected for demagnetizing effects, as the simple use of the geometrical factor $N=1$ for a plane is justified only for dense films with homogeneous magnetization. This is clearly not the case for the samples studied here. The correct demagnetizing factor cannot be given *ad hoc* and, therefore, the data are presented as a function of the applied field. Typical for all hysteresis loops is the strong difference in the measurements in the in-plane and out-of-plane directions. Due to the dominant *c*-axis texture and, therefore, the high degree of easy magnetization axis alignment, the out-of-plane measurements result in strong hysteretic, highly coercive loops, whereas the in-plane measurements result in narrow, flat magnetization loops with largely reduced coercivity and remanence. In all cases the susceptibility for the initial magnetization curve is large, indicating a nucleation dominated magnetization process. At low deposition temperatures the hysteresis loops show a shoulder at low magnetic fields. This shoulder could be either due to a soft magnetic phase (e.g., Fe), which, however, is not detected in XRD, or due to misaligned $Nd_2Fe_{14}B$ grains. The latter explanation is in agreement with the XRD measurements and also with the in-plane hysteresis, which is not completely narrow. The film deposited at 630 °C shows no shoulder in the magnetization loops and the in-plane loop is completely nonhysteretic. This sample possesses a perfect *c*-axis texture and a linear extrapolation of the in-plane loop results in an intersection with the out-of-plane measurement at $\mu_0 H_c = 6.8$ T, in very good agreement with the anisotropy field of the $Nd_2Fe_{14}B$ phase. A coercivity analysis after Kronmüller[24] had been performed and confirmed that domain nucleation is the dominating process responsible for magnetization reversal.[23] Furthermore, it revealed that nucleation is mainly initiated by large stray fields in these samples. For higher deposition temperatures the characteristic of the hysteresis changes again. The in-plane measurement remains narrow and nonhysteretic, an indication of good *c*-axis texture, the squareness of the out-of-plane loop is, however, strongly reduced. This suggests a rather inhomogeneous switching behavior, meaning a broad distribution of switching fields, which agrees with the observed large size distribution of the $Nd_2Fe_{14}B$ grains. It is also observed, that the overall magnetization values for samples deposited at higher temperatures are considerably lower. One possible explanation is the formation of an additional phase with lower saturation magnetization, which could also explain the unidentified reflection in the XRD pattern.

The magnetization in the remanent state, both perpendicular $M_r^{\perp}$ and parallel $M_r^{\parallel}$ to the film plane is summarized for different deposition temperatures in Fig. 5(a). Shown in the inset is the magnetization measured in an applied field of 4.5 T perpendicular to the substrate. Below 650 °C the values of around 0.8 T agree sufficiently well with the saturation magnetization of $Nd_2Fe_{14}B$ (1.61 T) considering a phase volume

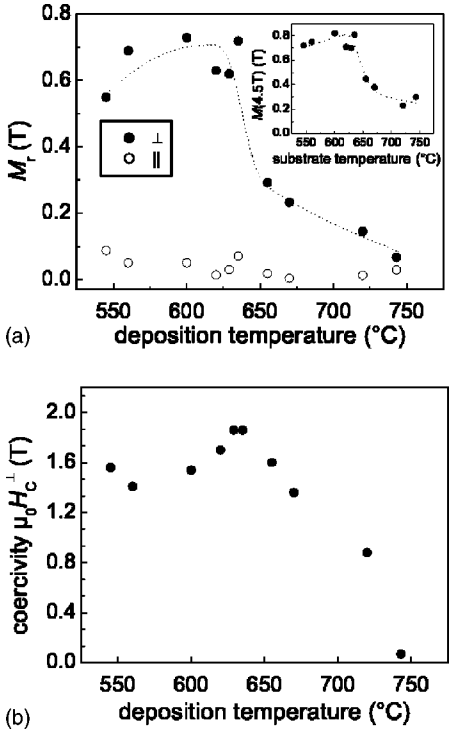

FIG. 5. Extrinsic magnetic properties of Nd-Fe-B films as a function of the deposition temperature. (a) Remanence measured perpendicular and parallel to the plane and magnetization measured perpendicular to the plane at a field of 4.5 T (in the inset). (b) Coercivity measured perpendicular to the plane.

of only 59% as estimated from the composition. For deposition at temperatures of 650 °C and above the magnetization drops significantly. The remanence perpendicular to the substrate reaches comparable values as the magnetization at 4.5 T, confirming the good out-of-plane texture of the films. Accordingly, the remanence in the film plane remains low for all deposition temperatures, with a minimum remanence ratio ($M_r^{\parallel}/M_r^{\perp}$) of 0.05. The coercivity of the films [Fig. 5(b)] stays on a high level of $\mu_0 H_c = 1.3-1.8$ T for substrate temperatures below 650 °C and then decreases substantially. The drop occurs at the same temperature as the drop in magnetization but there is not necessarily the same cause responsible for this behavior. A reduced coercivity can be explained considering the largely increased and inhomogeneous grain sizes observed for the $Nd_2Fe_{14}B$ grains forming at higher deposition temperatures. The large reduction of coercivity for deposition temperatures above 700 °C, however, is correlated with the onset of oxidation and the missing hard magnetic $Nd_2Fe_{14}B$ phase.

D. Magnetic domain structure

The magnetic domain images have been measured with the digital instruments dimension 3100 additionally to the topography in an interleave scan with a lift height of 100 nm. A commercial magnetic tip (MESP, Veeco Instruments) has been magnetized along the tip axis in the stray field of a strong Nd-Fe-B sinter magnet. Assuming a rigid tip magnetization (orientation) the measured phase shift of the cantilever oscillation is proportional to the second stray field derivative along the z axis (i.e., normal to the film plane):[25]

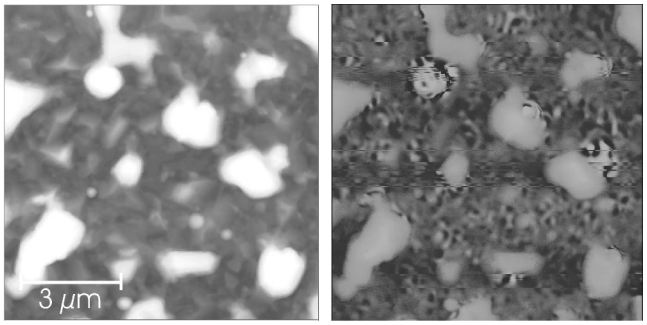

FIG. 6. Topography (left) and magnetic contrast as measured by MFM (right) for a Nd-Fe-B film deposited at 545 °C [same area as in Fig. 3(a)]. The MFM image clearly reveals the difference between the larger $Nd_2Fe_{14}B$ grains and the large nonmagnetic Nd particles.

$$\Delta\Phi \propto \frac{\partial^2 H_z}{\partial z^2}. \tag{1}$$

Whereas this would result in the imaging of domain walls in an idealistic point model (i.e., describing the magnetic coating as point dipole at the very tip end), for realistic cases of an extended tip the signal results from an integration of the above expression over the whole tip volume and therefore averages laterally over several 10 nm. Under these conditions a domain pattern of stripes of alternating magnetization perpendicular to the surface will be imaged by MFM as a similar pattern of dark and bright stripes. Hereby, a dark contrast (negative phase shift) equals a parallel alignment of tip and domain magnetization. The rigid tip assumption is not strictly valid in a quantitative sense (the volume of the tip, which is influenced by the stray field of the sample varies throughout the scan, depending mainly on the width and depth of the magnetic domain over which the tip is positioned),[25] but at least the direction of the tip magnetization remains unaltered during our measurements. This has been proved by scanning a representative area of the sample with two opposite initial magnetization directions of the tip. The phase contrast has essentially been reversed. All MFM measurements presented in the following have been performed on samples in the as-prepared, demagnetized state.

Figure 6 shows AFM and MFM measurements of the sample presented in Fig. 3(a). The AFM image matches exactly with the topographic image taken with the SEM. The MFM image shows a bright-dark contrast, which corresponds to magnetic domains with alternating magnetization perpendicular to the film, as explained in the beginning of the section. This contrast has a lateral scale of 150 nm and is found for the small $Nd_2Fe_{14}B$ grains composing the film. The small size, the irregular shape, and the direct contact does, however, not allow us to study the stray fields of individual grains. From the MFM measurements it is straightforward to distinguish between the Nd-rich grains, which show no magnetic contrast, and the similarly shaped larger $Nd_2Fe_{14}B$ grains (see again Fig. 3), which possess a strong and clear

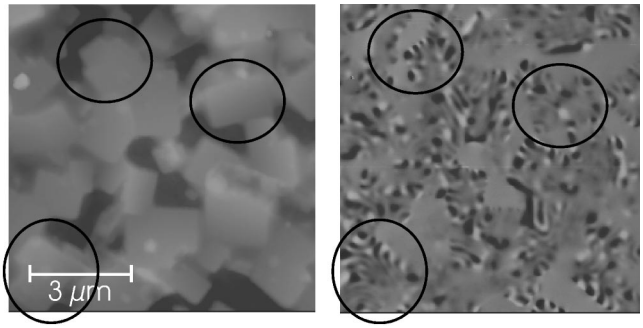

FIG. 7. Topography (left) and magnetic contrast as measured by MFM (right) for a Nd-Fe-B film deposited at 630 °C. Stripe domains and edge effects are clearly visible.

domain contrast. Interestingly, the domain width and also the measured phase contrast is larger in these grains, both of which are attributed to the larger dimensions. This interpretation will be elaborated in more detail later. The MFM images of the sample prepared at 630 °C (Fig. 7) nicely reflects the microstructure measured by AFM. Stripe domains are observed inside the rectangular $Nd_2Fe_{14}B$ grains, as expected for single-crystal particles with their easy axis perpendicular to the surface. In contrast, no domains are, of course, seen in regions where the Ta buffer layer remained blank. Compared to the previously discussed sample the larger size of the Nd–Fe–B grains (1–2 μm) allows us to see magnetic features in accordance to the geometric aspect of the particles, e.g., domain walls which end preferably perpendicular to grain edges. Another interesting observation is the stray field enhancement at a grain edge, an expected effect originating from the sharp boundary. This even leads to a situation where, in an overview image like Fig. 7 (right panel), some of the grains appear to possess magnetic domains only at the grain boundary. When zooming into a single grain, one also observes magnetic contrast in its center, however with reduced values. Figure 8 shows an MFM overview of the sample deposited at 670 °C. Stripe domains are revealed inside the $Nd_2Fe_{14}B$, but there is no contrast on the irregularly shaped Nd grains, which are sometimes found on top of the $Nd_2Fe_{14}B$ grains. The large rectangular grain to the left, which has been determined to be Nd rich [compare Fig. 3(b)] does not show any magnetic contrast. Although it was not possible to identify the actual phase of these grains, MFM

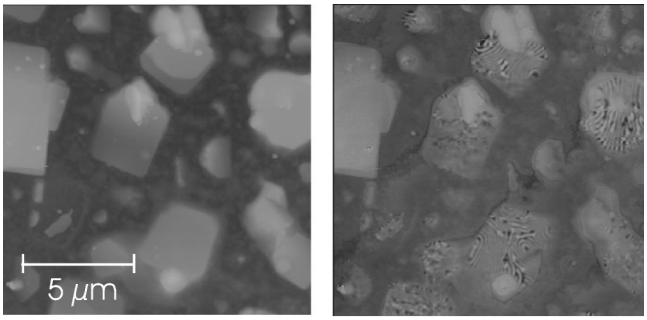

FIG. 8. Topography (left) and magnetic contrast as measured by MFM (right) for a Nd-Fe-B film deposited at 670 °C including the section from Fig. 3(b) and also the nonmagnetic grain.

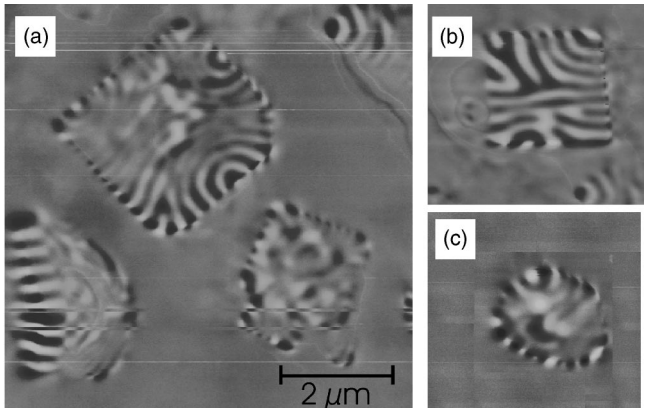

FIG. 9. Detailed domain structure for selected small (1–2 μm) $Nd_2Fe_{14}B$ grains. The scale is valid for all images. The domain size is about 150 nm.

clearly reveals the nonmagnetic nature at room temperature. Especially for higher deposition temperatures these grains constitute a large volume fraction of the magnetic film and can be made responsible for the reduced magnetization.

In these samples there exists the possibility to study the domain structure of isolated, geometrically well defined single-crystal particles with only a few microns in size. Figure 9 shows some examples of small sized grains. Again a stray field enhancement and a preferable orientation of domains perpendicular to the grain edges are observed. The domain width is on average 100–300 nm but it varies from grain to grain and can even change within a grain. An obvious reason for these variations in domain width are differences in the height of individual grains. For selected grains with regular shape and without visible defects the domain width was determined by MFM and the grain height by the corresponding AFM image. It appears that even regular looking grains are often wedge shaped [e.g., the grain in Fig. 9(b)] so that it has to be distinguished even between parts of a grain with different height. The experimental data of this study are plotted in Fig. 10. A general increase of domain width with grain height is observed. A comparison of this behavior with theoretical consideration would require a thorough micromagnetic simulation of different grains including all topographical features and seems to be beyond the ability of today's computer power. A rough understanding, however, is possible from domain theory of extended films with high perpendicular anisotropy. In this approach the domain configuration of an extended film of thickness D is simplified by parallel stripe domains with an alternating magnetization normal to the film plane. This model domain structure is sketched in the inset of Fig. 10. The domain width W results from minimizing the sum of stray field energy and wall energy. Applying the method by Kooy and Enz[26] to the present condition of zero net magnetization the following expression for the total energy (per unit area) is derived:[27]

$$E_{\mathrm{tot}} = E_{\mathrm{wall}} + E_d = \gamma_w/W + K_d D\left\{\frac{4p}{\pi^3}\sum_{n=\mathrm{odd}} n^{-3}\left[1-\left(1+\frac{2\pi n}{p}\right)\exp(-2\pi np)\right]\right\}. \quad (2)$$

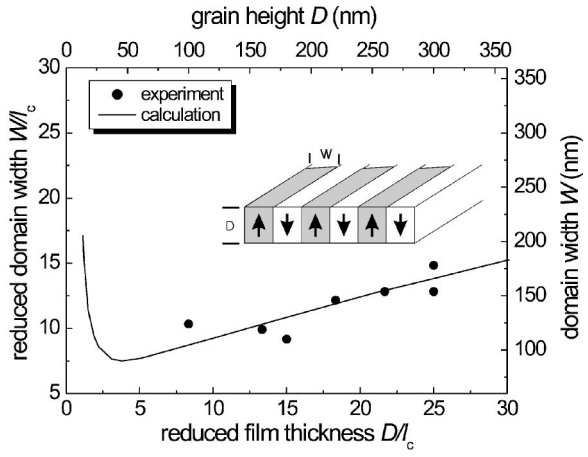

FIG. 10. Domain width W as a function of grain height D in absolute units and in units of $l_c=\gamma_w/2K_d=12$ nm. Measured data compared with calculation according to the theory of extended films.

Hereby $\gamma_w=4\sqrt{AK_u}$ denotes the wall energy, $K_d=J_s^2/2\mu_0$ denotes the stray field energy density constant, K_u and J_s are the uniaxial anisotropy constant and the saturation polarization, respectively, and $p=2W/D$ is a dimensionless parameter. The total energy density can be minimized with respect to p, leading to the expression,

$$\lambda_c=\frac{p^2}{\pi^3}\sum_{n=\text{odd}} n^{-3}\left[1-\left(1+\frac{2\pi n}{p}\right)\exp(-2\pi np)\right] \qquad (3)$$

with the normalized parameters $l_c=\gamma_w/2K_d, \lambda_c=l_c/D$. For a given value of p the corresponding λ_c can be calculated. Inverting the numerical solution results in W/l_c as a function of D/l_c. This function is plotted in Fig. 10 as a solid black line. The domain width decreases with reduced film thickness to a certain critical thickness of $4l_c$. For an even lower thickness D the domain width increases again.[28] On the second set of axes the same function is given in absolute values D and W, applying the result to $Nd_2Fe_{14}B$ (the wall energy γ_w and the stray field energy density K_d are 2.4×10^{-2} J/m^2 and 10^6 J/m^3 respectively, which leads to a value of $l_c\approx12$ nm). A very good agreement between the measured domain pattern and the prediction from domain theory of extended films is found. The large grain edge-to-height ratio of >10, which is found in these films, allows us to apply the simple domain theory to correctly describe the length scale of the investigated magnetic microstructure. The actual shape of the domain pattern, however, is influenced by the grain topography and shows the above mentioned finite size effects.

IV. CONCLUSIONS

In order to obtain excellent magnetic properties of Nd-Fe-B films prepared by direct deposition on heated substrates, proper phase formation and an appropriate microstructure are required. The substrate temperature must be sufficiently high for the formation of the highly anisotropic $Nd_2Fe_{14}B$ phase and should mediate a good alignment of the grains. The film properties are also largely influenced by the buffer material. An appropriate buffer must prevent interdiffusion and induce the intended texture. Additionally, the buffer must promote a suitable microstructure. Nd-Fe-B films were successfully prepared by pulsed laser deposition on epitaxial Ta buffer, which fulfill the above listed criteria. The careful study of the role of substrate temperature resulted in optimum film properties in a deposition temperature range between 600 °C and 650 °C. For low substrate temperatures small and irregular Nd and $Nd_2Fe_{14}B$ grains are formed on the Ta buffer and the intended texture is not fully developed. In the optimum deposition temperature range the $Nd_2Fe_{14}B$ phase grows epitaxially on the Ta (110) buffer and possesses a perfect (001) texture. The low wettability of $Nd_2Fe_{14}B$ and Nd on Ta results in a granular microstructure and isolated $Nd_2Fe_{14}B$ grains. The high mobility on this surface favors the formation of a regular habitus which reflects the tetragonal symmetry of the $Nd_2Fe_{14}B$ unit cell. The intrinsic properties of the $Nd_2Fe_{14}B$ phase present in the films are comparable to single-crystal properties.[20] Therefore, one can consider these films as an assembly of small micron-sized, rectangular $Nd_2Fe_{14}B$ single crystals. However, unlike bulk single crystals, which have insufficient extrinsic properties, these microcrystals are well separated from each other and show magnetization reversal at relatively high magnetic fields (almost 2 T). This is achieved by a regular shape and a low defect rate to avoid easy domain nucleation. On the other hand, the large stray fields which are imaged by MFM especially at sharp grain edges can facilitate domain nucleation and may limit coercivity. For higher deposition temperatures the microstructure coarsens substantially and oxidation leads to a destruction of the $Nd_2Fe_{14}B$ phase. Consequently, remanence and coercivity drop rapidly.

For medium deposition temperatures the combination of intrinsic magnetic properties and granular but regular microstructure does not only result in excellent extrinsic film properties, but allows one also to examine concepts of domain theory and micromagnetics not accessible up to now. The domain structure of micron-sized single-crystal $Nd_2Fe_{14}B$ grains has been investigated by magnetic force microscopy. The perpendicular uniaxial anisotropy and the small height of the grains lead to stripe domains, which are visible as a bright-dark contrast in the MFM image. The width of the stripe domains scales with the grain height in accordance to general domain theory of extended films. The details of the domains, however, resemble the actual shape of the grains. Domains end preferably perpendicular to grain edges and the stray field is enhanced at the sharp edges of these rectangular grains. This is a clear microscopic proof of the assumptions drawn from global magnetization measurements.

ACKNOWLEDGMENTS

The authors would like to thank Rudolf Schäfer for helpful discussions, Felix Zörgiebel for some MFM images, and the Deutsche Forschungsgemeinschaft for financial support through Grant No. SFB 463.

*Email address: v.neu@ifw-dresden.de

[1] A. Kruusing, Int. Mater. Rev. **44**, 121 (1999).
[2] L. Schultz and S. Fähler, in *Encyclopedia of Materials: Science and Technology*, edited by K. H. J. Buschow, R. W. Cahn, M. C. Flemings, B. Ilschner, E. J. Kramer, and S. Mahajan (Elsevier, Amsterdam, 2001).
[3] A. Melsheimer and H. Kronmüller, Physica B **299**, 251 (2001).
[4] A. S. Lileev, A. A. Parilov, and V. G. Blatov, J. Magn. Magn. Mater. **242-245**, 1300 (2002).
[5] M. Yu, Y. Liu, S. H. Liou, and D. J. Sellmyer, J. Appl. Phys. **83**, 6611 (1998).
[6] I. Panagiotopoulos and G. C. Hadjipanayis, Nanostruct. Mater. **10**, 1013 (1998).
[7] H. Jiang and M. J. Oshea, IEEE Trans. Magn. **37**, 2579 (2001).
[8] W. Liu, Z. D. Zhang, J. P. Liu, B. Z. Cui, X. K. Sun, J. Zhou, and D. J. Sellmyer, J. Appl. Phys. **93**, 8131 (2003).
[9] F. J. Cadieu, T. D. Cheung, L. Wickramasekara, and N. Kamprath, IEEE Trans. Magn. **22**, 752 (1986).
[10] D. J. Keavney, E. E. Fullerton, J. E. Pearson, and S. D. Bader, J. Appl. Phys. **81**, 4441 (1997).
[11] S. Parhofer, C. Kuhrt, J. Wecker, G. Gieres, and L. Schultz, J. Appl. Phys. **83**, 2735 (1998).
[12] V. Neu, U. Hannemann, S. Fähler, B. Holzapfel, and L. Schultz, J. Appl. Phys. **91**, 8180 (2002).
[13] U. Hannemann, S. Fähler, V. Neu, B. Holzapfel, and L. Schultz, IEEE Trans. Magn. **38**, 2805 (2002).
[14] L. K. E. B. Serrona, A. Sugimura, N. Adachi, T. Okuda, H. Ohsato, I. Sakamoto, A. Nakanishi, M. Motokawa, D. H. Ping, and K. Hono, Appl. Phys. Lett. **82**, 1751 (2003).
[15] L. Castaldi, H. A. Davies, and M. R. J. Gibbs, J. Magn. Magn. Mater. **242**, 1284 (2002).
[16] T. Shima, A. Kamegawa, K. Hono, and H. Fujimori, Appl. Phys. Lett. **78**, 2049 (2001).
[17] T. Okuda, A. Sugimura, O. Eryu, L. K. E. B. Seronna, N. Adachi, I. Sakamoto, and A. Nakanishi, Jpn. J. Appl. Phys. **42**, 6859 (2003).
[18] P. C. Gouteff, L. Folks, and R. Street, J. Magn. Magn. Mater. **177**, 1241 (1998).
[19] J. L. Tsai, T. S. Chin, Y. D. Yao, Z. G. Sun, B. G. Shen, and H. Kronmüller, IEEE Trans. Magn. **37**, 2582 (2001).
[20] U. Hannemann, S. Fähler, V. Neu, B. Holzapfel, and L. Schultz, Appl. Phys. Lett. **82**, 3710 (2003).
[21] U. Hannemann, S. Fähler, S. Oswald, B. Holzapfel, and L. Schultz, J. Magn. Magn. Mater. **242-245**, 1294 (2002).
[22] S. Fähler, U. Hannemann, S. Oswald, V. Neu, B. Holzapfel, and L. Schultz, IEEE Trans. Magn. **39**, 2950 (2003).
[23] U. Hannemann, S. Melcher, V. Neu, S. Fähler, B. Holzapfel, and L. Schultz, IEEE Trans. Magn. **39**, 2726 (2003).
[24] X. C. Kou, H. Kronmüller, D. Givord, and M. F. Rossignol, Phys. Rev. B **50**, 3849 (1994).
[25] J. Lohau, S. Kirsch, A. Carl, G. Dumpich, and E. F. Wassermann, J. Appl. Phys. **86**, 3410 (1999).
[26] C. Kooy and U. Enz, Philips Res. Rep. **15**, 7 (1960).
[27] See also A. Hubert and S. Schäfer, *Magnetic Domains* (Springer, Berlin, 1998), 306 ff.
[28] This is due to the compensation of magnetic poles on the top and bottom of the film, leading to a strong reduction of the stray field energy for small film thickness. As a consequence, the domain configuration results from the attempt of minimizing wall energy by increasing the domain width.